

THE RELATIVE ABUNDANCE OF ISOLATED CLUSTERS AS A PROBE OF DARK ENERGY

Jounghun Lee

*Department of Physics and Astronomy, FPRD, Seoul National University, Seoul 151-747,
Korea: jounghun@astro.snu.ac.kr*

ABSTRACT

Those galaxy clusters which do not belong to the superclusters are referred to as the isolated clusters. Their relative abundance at a given epoch may be a powerful constraint of the dark energy equation of state since it depends strongly on how fast the structures grow on the largest scale in the Universe. We note that the mass function of the isolated clusters can be separately evaluated through the modification of the recently developed Corasaniti-Achitouv (CA) theory according to which the stochastic collapse barrier is quantified by two coefficients: the drifting average coefficient (β) and the diffusion coefficient (D_B). Regarding β in the CA formalism as an adjustable parameter and assuming that the formation of isolated clusters corresponds to the case of $D_B = 0$, we determine the mass function of the isolated clusters by fitting the numerical results from the MICE simulations to the modified CA formula. It is found that the best-fit value of β changes with redshift and that the CA mass function with $D_B = 0$ agrees very well with the numerical results at various redshifts. Defining the relative abundance of the isolated clusters, ξ_I , as the ratio of the cumulative mass function of the isolated clusters to that of the non-isolated clusters at a given epoch, we finally show how sensitively ξ_I changes with the dark energy equation of state. It is also discussed how ξ_I can help to break the degeneracy between the dark energy equation of state and the other key cosmological parameters.

Subject headings: cosmology:theory — large-scale structure of universe

1. INTRODUCTION

The observed rich clusters of galaxies are believed to have formed through the gravitational collapse of the highest local peaks of the initial density field (Bardeen et al. 1986). Although most of the rich clusters belong to the larger-scale superclusters (e.g., Wray et al.

2006; Einasto et al. 2007), there exist few isolated massive clusters which reside in relatively low-density environments without having any close neighbor clusters. The relative abundance of the isolated clusters should depend on how strong the gravitational clustering is on the largest scale and how frequently the clusters merge into the superclusters in the Universe. Therefore, it is expected that the relative abundance of the isolated massive clusters may be useful to distinguish between different candidate dark energy models.

To predict the relative abundance of isolated clusters in different dark energy models, however, a theoretical framework is first required within which the number density of isolated clusters can be separately counted. The standard excursion set formalism has been conventionally employed to analytically calculate the number density of galaxy clusters as a function of mass, i.e., the mass function of galaxy clusters. Basically, the standard excursion set formalism counts the initial regions whose linearly extrapolated density contrast (δ) exceeds a fixed threshold value (δ_c) on a certain mass scale M , regarding them as the sites which would eventually collapse to form the bound objects of mass M (Press & Schechter 1974; Bond et al. 1991). The density threshold δ_c which is often called the *collapse barrier* has a constant value of $\delta_{sc} = 1.686$ if the gravitational collapse process follows the spherical dynamics (Gunn & Gott 1972).

Maggiore & Riotto (2010a,b) have for the first time introduced the concept of the stochastic collapse barrier to generalize the excursion set formalism. In the light of the numerical result of Robertson et al. (2009), Maggiore & Riotto (2010a,b) regarded the collapse barrier, δ_c , as a log-normal variable, and showed that in the high-mass limit the collapse barrier has a spherical average of $\langle \delta_c \rangle = \delta_{sc} = 1.686$. Very recently, Corasaniti & Aчитouv (2011a,b) have made a further refinement of the mass function theory by incorporating the ellipsoidal collapse dynamics into the generalized excursion set formalism. They extended the generalized excursion set formalism to the case that the mean collapse barrier, $\langle \delta_c \rangle$, deviates from the spherical average, $\delta_{sc} = 1.686$ in the low-mass limit. The higher collapse barrier than the spherical average, $\delta_c > 1.686$, corresponds to the case that the formation of the low-mass halos experience the disturbing tidal effect from the surroundings.

We note here that the Corasaniti-Aчитouv formalism should be applicable not only to the case that the gravitational collapse occurs non-spherically in the low-mass section but also to the case that the massive halos form in isolated low-density environments. Given that the massive cluster-size halos are likely to form in the highly overdense regions but hardly in the isolated low-density regions, the collapse barrier for the formation of the isolated clusters should be higher than the spherical average. Since the Corasaniti-Aчитouv formalism allows the average collapse barrier to deviate from the spherical value of 1.686, their formalism may be capable of deriving the mass function of the isolated clusters.

The organization of this paper is as follows. In §2 we briefly review the Corasaniti-Achitouv formalism of the halo mass function. In §3 we explain how the relative abundance of the isolated clusters can be evaluated by modifying the Corasaniti-Achitouv formalism and present the results of the numerical tests. In §4 we show how sensitively the relative abundance of the isolated clusters depends on the dark energy equation of state as well as the other key cosmological parameters. §5 we summarize the results and conclude the work.

2. THE CORASANITI-ACHITOUV FORMALISM

The mass function of bound halos, $dN/d\ln M$, is defined as the number density of the bound objects whose masses belong to the differential mass interval $[\ln M, \ln M + d\ln M]$ (Press & Schechter 1974). The classical mass function theory based on the standard excursion set formalism relates $dN/d\ln M$ to the multiplicity function, $f(\sigma)$, which gives the number density of the random-walks crossing a specified collapse barrier, δ_c , when the pseudo time variable has the value of σ (Bond et al. 1991; Jedamzik 1995):

$$\frac{dN(M, z)}{d\ln M} = \frac{\bar{\rho}}{M} \frac{d\ln \sigma^{-1}}{d\ln M} f[\sigma(M, z)]. \quad (1)$$

Here $\bar{\rho}$ is the mean mass density of the Universe and the pseudo time variable $\sigma(M, z)$ is equivalent to the rms density fluctuation of the linear density field smoothed on the mass scale M at redshift z . It scales with the linear growth factor, $D(z)$, as $\sigma(M, z) \equiv D(z)\sigma(M)$ with $\sigma(M) \equiv \sigma(M, z=0)$. Throughout §2 and §3, we assume a flat Λ CDM cosmology (with $\Omega_m = 0.25$, $\Omega_\Lambda = 0.75$, $\Omega_b = 0.045$, $h = 0.7$, $n_s = 0.95$ and $\sigma_8 = 0.8$), for which the linear growth factor has the following analytical expression (Lahav et al. 1991):

$$D(z) \propto \frac{5}{2} \Omega_m [\Omega_m (1+z)^3 + \Omega_\Lambda]^{1/2} \int_z^\infty dz' \frac{1+z'}{[\Omega_m (1+z')^3 + \Omega_\Lambda]^{3/2}}. \quad (2)$$

Here $D(z)$ is normalized to satisfy $D(z=0) = 1$.

In the original Press-Schechter theory where the gravitational collapse is assumed to occur spherically, the collapse barrier has a constant value of $\delta_{sc} = 1.686$. In the Press-Schechter variants developed afterward to improve the accuracy of the halo mass function by accounting for the ellipsoidal collapse process (e.g., Bond & Myers 1996; Monaco 1997; Audit et al. 1997; Lee & Shandarin 1998; Sheth & Tormen 1999; Jenkins et al. 2001; Warren et al. 2006; Tinker et al. 2008; Robertson et al. 2009), the collapse barrier is described not as a constant but as a function of the mass scale M (or equivalently, a function of the rms density fluctuation, σ).

Recently, Maggiore & Riotto (2010a,b, hereafter MR10) pointed out that not only the constant spherical collapse barrier but also the scale-dependent ellipsoidal collapse barrier is incapable of describing the true nature of the complicated halo formation process and suggested that the collapse barrier δ_c should be treated as a stochastic variable. MR10 derived an analytic expression for the halo mass function by generalizing the excursion set formalism for the case that the collapse barrier is stochastic and the random walk process is non-Markovian. It was shown by MR10 that in the high-mass limit ($M \geq 10^{14} h^{-1} M_\odot$) the average of the stochastic collapse barrier equals the constant spherical value, $\langle \delta_c \rangle = \delta_{sc} = 1.686$ and its variance is scale-dependent as $\langle \Delta^2 D_B \rangle = \sigma^2(M) D_B$ where D_B is called the diffusion coefficient. The stochasticity of the collapse barrier is caused by the disturbance from the surroundings and the ambiguity in the halo-identification procedure (see Maggiore & Riotto 2010b, for a detailed explanation).

In the light of the MR10 work, Corasaniti & Achitouv (2011a,b, hereafter CA11) have extended the generalized excursion set formalism to the ellipsoidal collapse case in which the average of δ_c deviates from the spherical value, 1.686, in the low-mass section. The resulting CA11 multiplicity function has two characteristic coefficients: the diffusion coefficient D_B defined as in the MR10 formalism and the drifting average coefficient, β , defined as $\langle \delta_c \rangle \equiv \delta_{sc} + \beta$. The non-zero value of this drifting average coefficient, β , quantifies the degree of the deviation of the average of the collapse barrier from the spherical average 1.686, while the non-zero value of the diffusion coefficient D_B quantifies the degree of the stochasticity of the collapse barrier δ_c .

The CA11 multiplicity function $f(\sigma)$ was written at second order as

$$f(\sigma; D_B, \beta) \approx f^{(0)}(\sigma; D_B) + f_{\beta=0}^{(1)}(\sigma; D_B) + f_{\beta}^{(1)}(\sigma; D_B) + f_{\beta^2}^{(1)}(\sigma; D_B), \quad (3)$$

where

$$f^{(0)}(\sigma; D_B) = \frac{\delta_{sc}}{\sigma \sqrt{1 + D_B}} \sqrt{\frac{2}{\pi}} e^{-\frac{(\delta_{sc} + \beta \sigma^2)^2}{2\sigma^2(1 + D_B)}}, \quad (4)$$

$$f_{\beta=0}^{(1)}(\sigma; D_B) = -\tilde{\kappa} \frac{\delta_{sc}}{\sigma} \sqrt{\frac{2a}{\pi}} \left[e^{-\frac{a\delta_{sc}^2}{2\sigma^2}} - \frac{1}{2} \Gamma(0, x) \right], \quad (5)$$

$$f_{\beta}^{(1)}(\sigma; D_B) = -\beta a \delta_{sc} \left[f_{\beta=0}^{(1)}(\sigma) + \tilde{\kappa} \text{Erfc}(x) \right], \quad (6)$$

$$f_{\beta^2}^{(1)}(\sigma; D_B) = \beta^2 a^2 \delta_{sc}^2 \tilde{\kappa} \left\{ \text{Erfc}(x) + \frac{\sigma}{a \delta_{sc}} \sqrt{\frac{a}{2\pi}} \left[e^{-\frac{a\delta_{sc}^2}{2\sigma^2}} \left(\frac{1}{2} - 2x \right) + \frac{3}{4} \frac{a \delta_{sc}^2}{\sigma^2} \Gamma(0, x) \right] \right\}, \quad (7)$$

with $x \equiv (\delta_{sc}/\sigma) \sqrt{a/2}$, $a = 1/(1 + D_B)$, $\tilde{\kappa} = \kappa a$, $k = 0.475$, and incomplete Gamma function $\Gamma(0, x)$. Here, $f^{(0)}(\sigma; D_B)$ coincides with the MR10 multiplicity function which has only one parameter D_B . Computing the halo mass functions through Equations (1)-(7) and comparing them with the fitting formula given by Tinker et al. (2008), CA11 have

determined the best-fit values of the two coefficients as $\beta = 0.057$ and $D_B = 0.294$. CA11 have also shown how the shape of the halo mass function changes with the values of D_B and β (see Figure 3 in Corasaniti & Achitouv 2011b). According to their results, the variation of the diffusion coefficient D_B alters the high-end slope of $f(\sigma)$ while the variation of the drifting average coefficient β affects the over-all amplitude of $f(\sigma)$.

Now, we would like to confirm the validity of the CA11 mass function by testing it against the high-resolution MICE simulations (Crocce et al. 2010) which traced the evolution of 2048^3 dark matter particles (each having mass of $23.42 \times 10^{10} h^{-1} M_\odot$) on a periodic box with linear size of $3 h^{-1} \text{Gpc}$ for a ΛCDM cosmology. We utilize the publicly available catalog of the cluster halos that were identified via the standard Friends-of-Friends (FoF) algorithm. The catalog provides information on each halo’s (comoving) position, peculiar velocity and FoF mass (calculated as the sum of the masses of all the dark matter particles belonging to each halo) at three different redshifts: $z = 0, 0.5, 1$. For a detailed description of the MICE simulations and the cluster catalogs, we refer the readers to Crocce et al. (2010).

Binning the logarithmic masses of the cluster halos from the MICE catalog and counting the number densities of the cluster halos belonging to each logarithmic mass-bin, we obtain the numerical mass function of all cluster halos, $dN_T/d\ln M$, at each redshift. Fitting the CA11 formula (Eqs [1]-[7]) to the numerical results from the MICE simulations at each redshift, we have determined the best-fit values of β and D_B with the help of the χ^2 statistics, the results of which are listed in Table 1.

Note that the diffusion coefficient, D_B , has the same best-fit value of 0.38 at all three redshifts while the best-fit value of the drifting average coefficient, β , increases as the redshift decreases. The result indicates that at earlier epochs the gravitational collapse process is closer to the spherical dynamics than at present epoch. Since a bound halo is harder to form at earlier epochs, those high- z halos must correspond to higher peaks in the initial density field. As shown analytically by Bernardeau (1994), the higher a local density peak is, the more spherically its gravitational collapse proceeds.

It is also worth mentioning that our result on the best-fit value of $D_B = 0.38$ is different from the original value $D_B = 0.27$ used in the CA11 formalism. This discrepancy must be due to the fact that we use the FoF masses available in the MICE catalog while the spherical over-density (SO) masses were considered in the original CA11 work.

Figure 1 plots the CA11 mass functions with the best-fit values of β and D_B (solid line) and compare them with the numerical results from the MICE simulations (square dots) at $z = 0, 0.5$ and 1 in the top-left, top-middle and top-right panels, respectively. The Jackknife method is employed to calculate the errors: Dividing the halos into eight subsamples (each

having the same number of the halos) and determining $dN_T/d\ln M$ separately from each subsample, the errors are calculated as one σ scatter of $dN_T/d\ln M$ among the eight Jackknife resamples. Figure 1 also plots the ratio of the analytic mass function to the numerical result as a function of mass at $z = 0, 0.5$ and 1 in the bottom-left, bottom-middle and bottom-right panel, respectively. As can be seen, the analytical and numerical mass functions agree with each other quite at all three redshifts, except in the high-mass section ($M > 10^{15} h^{-1} M_\odot$) where the Jackknife errors are very large.

3. MASS FUNCTION OF THE ISOLATED CLUSTERS

Applying the FoF algorithm with the linkage length parameter of b to the MICE cluster catalogs at each redshift, we first find the clusters of clusters (i.e., superclusters) which have more than one neighbor clusters within the FoF linkage length, $b\bar{l}$ where \bar{l} is the mean cluster separation. The *isolated clusters* are then identified as those clusters which do not belong to any superclusters. Note that the degree of their isolation depends on the value of b : The larger the value of b is, the more isolated they are. Here we consider the extreme case in which the isolated clusters experience no disturbance from the surrounding large-scale structures and the difference between their FoF and SO masses is negligible. In this extreme case, the value of the diffusion coefficient, D_B , must vanish since the non-zero value of D_B indicates the presence of the disturbance from the surroundings and the existence of the difference between the FoF and SO masses.

The ad-hoc value of the linkage length parameter for this extreme case is determined to be $b = 0.4$ by the following procedures. We first investigate how the best-fit value of D_B changes as the value of b varies from 0.25 to 0.45 in the FoF algorithm applied to the MICE cluster catalogs. For each case of b , we select the isolated clusters from the MICE cluster catalog and obtain the numerical mass function of the isolated clusters. Then, we fit the numerical result to the analytic CA11 formula (Eq.[1]-[7]) to determine the best-fit values of D_B and β with the help of the χ^2 statistics. Figure 2 plots the best-fit value of D_B versus the linkage length parameter b . As can be seen, the best-fit value of D_B drops to zero when the linkage length parameter b reaches up to 0.4. Table 2 lists the best-fit values of D_B and β for the mass function of the isolated clusters when the ad-hoc value of the linkage length parameter is set at $b = 0.4$.

Now, we write the total mass function of all cluster halos, $dN_T/d\ln M$, as the sum of the mass function of the isolated cluster halos, $dN_I/d\ln M$ and that of the non-isolated cluster

halos, $dN_{\text{NI}}/d \ln M$:

$$\frac{dN_T(M, z)}{d \ln M} = \frac{dN_I(M, z)}{d \ln M} + \frac{dN_{\text{NI}}(M, z)}{d \ln M}. \quad (8)$$

Putting $D_B = 0$ in the CA11 formula, we express the mass function of the isolated clusters as

$$\frac{dN_I(M, z)}{d \ln M} = \frac{\bar{\rho}}{M} \frac{d \ln \sigma^{-1}}{d \ln M} f[\sigma; \beta, D_B = 0]. \quad (9)$$

Here the multiplicity function of the isolated clusters which is characterized by one coefficient β is written at second order as

$$f(\sigma; D_B = 0, \beta) \approx f^{(0)}(\sigma) + f_{\beta=0}^{(1)}(\sigma) + f_{\beta}^{(1)}(\sigma) + f_{\beta^2}^{(1)}(\sigma), \quad (10)$$

where

$$f^{(0)}(\sigma) = \frac{\delta_{sc}}{\sigma} \sqrt{\frac{2}{\pi}} e^{-\frac{(\delta_{sc} + \beta \sigma^2)^2}{2\sigma^2}}, \quad (11)$$

$$f_{\beta=0}^{(1)}(\sigma) = -\kappa \frac{\delta_{sc}}{\sigma} \sqrt{\frac{2}{\pi}} \left[e^{-\frac{\delta_{sc}^2}{2\sigma^2}} - \frac{1}{2} \Gamma(0, x) \right], \quad (12)$$

$$f_{\beta}^{(1)}(\sigma) = -\beta \delta_{sc} \left[f_{\beta=0}^{(1)}(\sigma) + \kappa \text{Erfc}(x) \right], \quad (13)$$

$$f_{\beta^2}^{(1)}(\sigma) = \beta^2 \delta_{sc}^2 \kappa \left\{ \text{Erfc}(x) + \frac{\sigma}{\delta_{sc}} \sqrt{\frac{1}{2\pi}} \left[e^{-\frac{\delta_{sc}^2}{2\sigma^2}} \left(\frac{1}{2} - 2x \right) + \frac{3}{4} \frac{\delta_{sc}^2}{\sigma^2} \Gamma(0, x) \right] \right\}. \quad (14)$$

Figure 3 plots the analytical mass functions of the isolated clusters (solid lines) with the best-fit values of β and compared them with the numerical results from the MICE simulations (square dots) at $z = 0, 0.5$ and 1 in the top-left, top-middle and top-right panel, respectively. As can be seen, the analytical mass functions of the isolated clusters agree quite well with the numerical results at all three redshifts. The ratios of the analytic CA11 formula to the numerical results are plotted in the bottom panels. Although the agreements between the analytical and the numerical results for the case of the isolated clusters are not so excellent as for the case of all cluster halos (see Figure 1), the ratio at each redshift is still quite close to unity: the discrepancy is less than 20% except in the high-mass limit where the Jackknife errors are very large.

This result indicates that the CA11 formula with $D_B = 0$ indeed works fairly well for the determination of the mass function of the isolated clusters. It is worth emphasizing here that this analytical mass function of the isolated clusters (Eq. [9]) has only one coefficient β and there is no fitting normalization constant. The amplitude of $dN_I/d \ln M$ is found to automatically match the numerical result when the best-fit value of β is put into the CA formula.

Figure 4 plots the ratio of the mass function of the isolated clusters to that of the non-isolated clusters at $z = 0, 0.5$ and 1 in the left, middle and right panel, respectively. The errors are calculated as one σ scatter of the ratio among the eight Jackknife resamples. As can be seen, the numerical result (square dots) agrees fairly well with the analytic prediction (solid line) based on the CA11 formula at each redshift. We believe that it would reduce the existing discrepancy between the analytical and numerical results even more to include the higher order terms in the calculation of the multiplicity function, $f(\sigma; D_B, \beta)$. Throughout this paper, however, we consider only the second order approximation of $f(\sigma; D_B, \beta)$. Note that the ratio drops with mass more rapidly at higher redshifts, indicating that at high redshifts most of the very massive clusters have stronger tendency to form in the highly overdense regions than at present epoch.

4. DEPENDENCE ON THE DARK ENERGY EQUATION OF STATE

In a Λ CDM cosmology the dark energy equation of state (defined as the ratio of the pressure density to the energy density) is a perfect constant given as $w \equiv P_\Lambda/\rho_\Lambda = -1$. Whereas in dynamic dark energy

models the value of w may vary with time and can deviate from -1 at $z = 0$ (Wang & Steinhardt 1998). This difference in the dark energy equation of state results in the different functional shape of $D(z)$ (Chevallier & Polarski 2001; Linder 2003; Basilakos 2003; Percival 2005).

The evolution of the abundance of galaxy clusters has been regarded as one of the most powerful probes of $w(z)$ (e.g., Wang & Steinhardt 1998; Haiman et al. 2001; Weller et al. 2002). The most serious systematics in constraining $w(z)$ with the evolution of the abundance of the galaxy clusters may come from the mass assignment of the high- z clusters. Several statistical methods have been suggested so far to overcome the systematics but none of them have yet to be fully satisfactory (e.g., Rykoff et al. 2008; Cunha & Evrard 2010; Stanek et al. 2010, and references therein). See also Allen et al.(2011) for the latest review. We suggest here that the relative abundance of the galaxy clusters at a given epoch provides a complimentary probe of the dark energy equation of state.

The relative abundance of the isolated clusters is defined as the ratio of the cumulative mass function of the isolated clusters to that of the non-isolated clusters:

$$\xi_I(M_c; z) \equiv \left[\int_{M_c}^{\infty} d \ln M \frac{dN_I(M, z)}{d \ln M} \right] / \left[\int_{M_c}^{\infty} d \ln M \frac{dN_{NI}(M, z)}{d \ln M} \right], \quad (15)$$

where the mass function of the non-isolated cluster $dN_{NI}/d \ln M$ is obtained by $dN_T/d \ln M - dN_I/d \ln M$. To demonstrate how the relative abundance of the isolated clusters ξ_I changes

with the dark energy equation state w , we consider the specific case where the dark energy equation of state is redshift dependent as $w(z) = w_0 + w_1 z / (1 + z)$ (Chevallier & Polarski 2001; Linder 2003). Basilakos (2003) and Percival (2005) showed that for these dynamic dark energy models the linear growth factor can be approximated as:

$$D(z) = \frac{5\Omega_{mz}}{2(z+1)} \left[\Omega_{mz}^\alpha - \Omega_{Qz} + \left(1 + \frac{\Omega_{mz}}{2} \right) (1 + \mathcal{A}\Omega_{Qz}) \right]^{-1}, \quad (16)$$

where

$$\alpha = \frac{3}{5 - 2/(1 - w)} + \frac{3}{125} \frac{(1 - w)(1 - 3w/2)}{(1 - 6w/5)^3} [1 - \Omega_{mz}], \quad (17)$$

$$\mathcal{A} = -\frac{0.28}{w + 0.08} - 0.3. \quad (18)$$

Here Ω_{mz} and Ω_{Qz} represent the matter density and dark energy density parameters at z , respectively, related to their present values, Ω_m and Ω_Q as

$$\Omega_{mz} = \frac{\Omega_m(1+z)^3}{E^2(z)}, \quad \Omega_{Qz} = \frac{\Omega_Q}{E^2(z)(1+z)^{f(z)}}. \quad (19)$$

where

$$E^2(z) = \Omega_m(1+z)^3 + \Omega_Q(1+z)^{-f(z)}, \quad (20)$$

$$f(z) = -3(1 + w_0) - \frac{3w_1}{2 \ln(1 + z)}. \quad (21)$$

We first calculate ξ_I for the Λ CDM case and then repeat the calculation of ξ_I for the four different dynamic dark energy models at $z = 0.5$. Figure 5 plots the relative abundances of the isolated clusters for the dynamic dark energy models and compare them with the Λ CDM case. The errors for the Λ CDM case are calculated as one σ scatter of ξ_I among the eight Jackknife resamples from the MICE cluster catalog. As can be seen, the five different dark energy models predict different relative abundances of the isolated clusters. For the case of $w_1 > 0$ ($w_1 < 0$), the relative abundance of the isolated clusters has lower (higher) amplitude than for the Λ CDM case. This can be explained by the following logic. In a dark energy model with $w_1 > 0$ ($w_1 < 0$) the largest-scale powers are higher (lower) than in the Λ CDM case and thus boost the merging of the isolated clusters into the superclusters, reducing the relative abundance of the isolated clusters.

Furthermore, the differences in ξ_I between each dynamic dark energy case and the Λ CDM case are larger than the statistical errors calculated through the Jackknife resampling. If a future cluster survey can find as many clusters as the MICE simulations, the sensitivity

shown in Figure 5 suggests that the relative abundance of the isolated clusters will be a powerful probe of the dark energy equation of state in practice.

We examine the degeneracy between w_0 and w_1 . Varying the value of w_0 from -1 to -0.9 and the value of w_1 from -0.6 to 0.6 , we repeatedly calculate ξ_I at $z = 0.5$, setting the cutoff mass scale at $M_c = 3.35 \times 10^{13} h^{-1} M_\odot$ (the lowest cluster mass in the MICE catalog). The contour curves of ξ_I in the w_0 - w_1 plane are plotted in Figure 6. When w_0 is fixed, the relative abundance of the isolated clusters decreases as the value of w_1 increases, which is consistent with Figure 5.

We also examine the degeneracy between Ω_m and w_1 and between σ_8 and w_1 at $z = 0.5$, which are plotted in the left and right panels of Figure 7, respectively. For these plots the value of w_0 is set at -1 . As can be seen, when w_1 is fixed, the relative abundance of the isolated clusters, ξ_I , increases as the value of Ω_m increases. This implies that if there is stronger gravitational effect due to the larger amount of dark matter, the formation of a cluster can occur more easily even in isolated low-density environments. For a given value of ξ_I , w_1 increases with Ω_m . A similar trend is found in the σ_8 - w_1 degeneracy curves. When w_1 is fixed, ξ_I increases as the value of σ_8 increases. The overall high density powers make it less hard for a cluster to form in the isolated low-density environments.

It is worth mentioning here that the degeneracy trends shown in Figures 6-7 are different from those obtained from the total cluster abundance (see Wang & Steinhardt 1998; Weller et al. 2002). The increase of w_1 has the same effect on the cluster abundance as the increase of Ω_m and σ_8 : the cluster abundance increases as the three parameters increase. In contrast, when the relative abundance of isolated clusters is used, the increase of w_1 has the opposite effect: The relative abundance of the isolated clusters increases as w_1 decreases and as Ω_m and σ_8 increase. This result implies that the relative abundance of the isolated clusters may be helpful to break the degeneracy between w_1 and the other key cosmological parameters.

5. SUMMARY AND DISCUSSION

We have derived the mass function of the isolated clusters in the frame of the recently developed Corasaniti-Achitouv formalism, assuming that for the case of the isolated clusters there is no disturbance from the surroundings and no ambiguity in the mass determination. The numerical results from the MICE simulations have been used to determine empirically the value of the drifting average coefficient, β , which quantifies the degree of the deviation of the collapse barrier for the formation of the isolated clusters from the standard average

value.

Extrapolating the validity of the Corasaniti-Achitouv formalism to the dynamic dark energy models and using our analytic result on the mass function of the isolated clusters, we have shown that the relative abundance of the isolated clusters, ξ_I , defined as the ratio of the cumulative mass function of the isolated clusters to that of the non-isolated clusters at a given epoch, depends sensitively on the dark energy equation of state. This result proves our theoretical concept that the relative abundance of the isolated clusters is in principle a powerful probe of dark energy.

Yet, several additional works have to be done before constraining the dark energy equation of state with ξ_I . First, it will be necessary to derive the functional form of the drifting average coefficient, $\beta(z)$, for the isolated and non-isolated cases, separately. Second, it has to be confirmed if the Corasaniti-Achitouv formalism indeed works not only in a Λ CDM cosmology but also in dynamic dark energy models and how the drifting average coefficient changes with the background cosmology. Third, it has to be examined whether or not the higher-order perturbation terms in the Corasaniti-Achitouv formalism have any non-negligible effect on the relative abundance of the isolated clusters. We plan to conduct these works and wish to report the results elsewhere in the future.

We would also like to mention that our analytic model for the mass function of the isolated clusters will be useful not only as a probe of dark energy equation of state but also for predicting more accurately the cluster-related statistics since the isolated massive clusters may differ from the non-isolated ones in their physical properties such as average shape, dynamical state, gas entropy profile and etc (in private communication with E.Komatsu).

I thank a referee for helpful suggestions and E. Komatsu for stimulating discussion. I acknowledge the use of data from the MICE simulations that are publicly available at <http://www.ice.cat/mice>. I also acknowledge the financial support from the National Research Foundation of Korea (NRF) grant funded by the Korea government (MEST, No.2011-0007819) and from the National Research Foundation of Korea to the Center for Galaxy Evolution Research.

REFERENCES

- Allen, S. W., Evrard, A. E., & Mantz, A. B. 2011, arXiv:1103.4829
- Audit, E., Teyssier, R., & Alimi, J. M. 1997, A&A, 325, 439
- Basilakos, S. 2003, ApJ, 590, 636
- Basilakos, S., Plionis, M., & Lima, J. A. S. 2010, Phys. Rev. D, 82, 083517
- Bardeen, J. M., Bond, J. R., Kaiser, N., & Szalay, A. S. 1986, ApJ, 304, 15
- Bernardeau, F. 1994, ApJ, 427, 51
- Bond, J. R., Cole, S., Efstathiou, G., & Kaiser N. 1991, ApJ, 379, 440
- Bond, J. R., & Myers, S. T. 1996, ApJS, 103, 1
- Chevallier, M. & Polarski, D. 2001, Int. J. Mod. Phys. D, 10, 213
- Corasaniti, P. S., & Achitouv, I. 2011, Physical Review Letters, 106, 241302
- Corasaniti, P. S., & Achitouv, I. 2011, arXiv:1107.1251
- Crocce, M., Fosalba, P., Castander, F. J., & Gaztañaga, E. 2010, MNRAS, 403, 1353
- Cunha, C. E., & Evrard, A. E. 2010, Phys. Rev. D, 81, 083509
- Davis, M., Efstathiou, G., Frenk, C. S., & White, S. D. M. 1985, ApJ, 292, 371
- Einasto, J., et al. 2007, A&A, 462, 811
- Eke, V. R., Cole, S., & Frenk, C. S. 1996, MNRAS, 282, 263
- Gunn, J. E., & Gott, J. R., III 1972, ApJ, 176, 1
- Haiman, Z., Mohr, J.J. & Holder, G.P. 2001, ApJ, 553, 545
- Jedamzik, K. 1995, ApJ, 448, 1
- Jenkins, A., et al. 2001, MNRAS, 321, 372
- Jones, M., et al. 1993, Nature, 365, 320
- Kasun, S. F., & Evrard, A. E. 2005, ApJ, 629, 781
- Komatsu, E., et al. 2011, ApJS, 192, 18

- Lahav, O., Lilje, P. B., Primack, J. R., & Rees, M. J., 1991, MNRAS, 251, 128
- Lee, J. & Shandarin, S. F. 1998, ApJ, 500, 14
- Lee, J., & Evrard, A. E. 2007, ApJ, 657, 30
- Linder, E. 2003, Phys. Rev. Lett., 90, 091301
- Linder, E. V. 2005, Phys. Rev. D, 72, 043529
- Lue, A., Scoccimarro, R., & Starkman, G. D. 2004, Phys. Rev. D, 69, 124015
- Maggiore, M., & Riotto, A. 2010, ApJ, 711, 907
- Maggiore, M., & Riotto, A. 2010, ApJ, 717, 515
- Maggiore, M., & Riotto, A. 2010, ApJ, 717, 526
- Monaco, P. 1997, MNRAS, 290, 439
- Percival, W. J. 2005, A&A, 819, 830
- Press, W. H., & Schechter, P. 1974, ApJ, 187, 425
- Reed, D., Gardner, J., Quinn, T., Stadel, J., Fardal, M., Lake, G., & Governato, F. 2003, MNRAS, 346, 565
- Robertson, B. E., Kravtsov, A. V., Tinker, J., & Zentner, A. R. 2009, ApJ, 696, 636
- Rykoff, E. S., et al. 2008, MNRAS, 387, L28
- Sheth, R. K., & Tormen, G. 1999, MNRAS, 308, 119
- Sheth, R. K., Mo, H., & Tormen, G. 2001, MNRAS, 323, 1
- Springel, V., White, M., & Hernquist, L. 2001, ApJ, 549, 681
- Springel, V., et al. 2005, Nature, 435, 629
- Stanek, R., Rasia, E., Evrard, A. E., Pearce, F., & Gazzola, L. 2010, ApJ, 715, 1508
- Tinker, J. L., et al. 2008, ApJ, 688, 709
- Wang, L. & Steinhardt, P. J. 1998, ApJ, 508, 483
- Warren, M. S., Abazajian, K., Holz, D. E., & Teodoro, L. 2006, ApJ, 646, 881

Weller, J., Battye, R. A., & Kneissl, R. 2002, Phys. Rev. Lett., 88, 231301

Wray, J. J., Bahcall, N. A., Bode, P., Boettiger, C., & Hopkins, P. F. 2006, ApJ, 652, 907

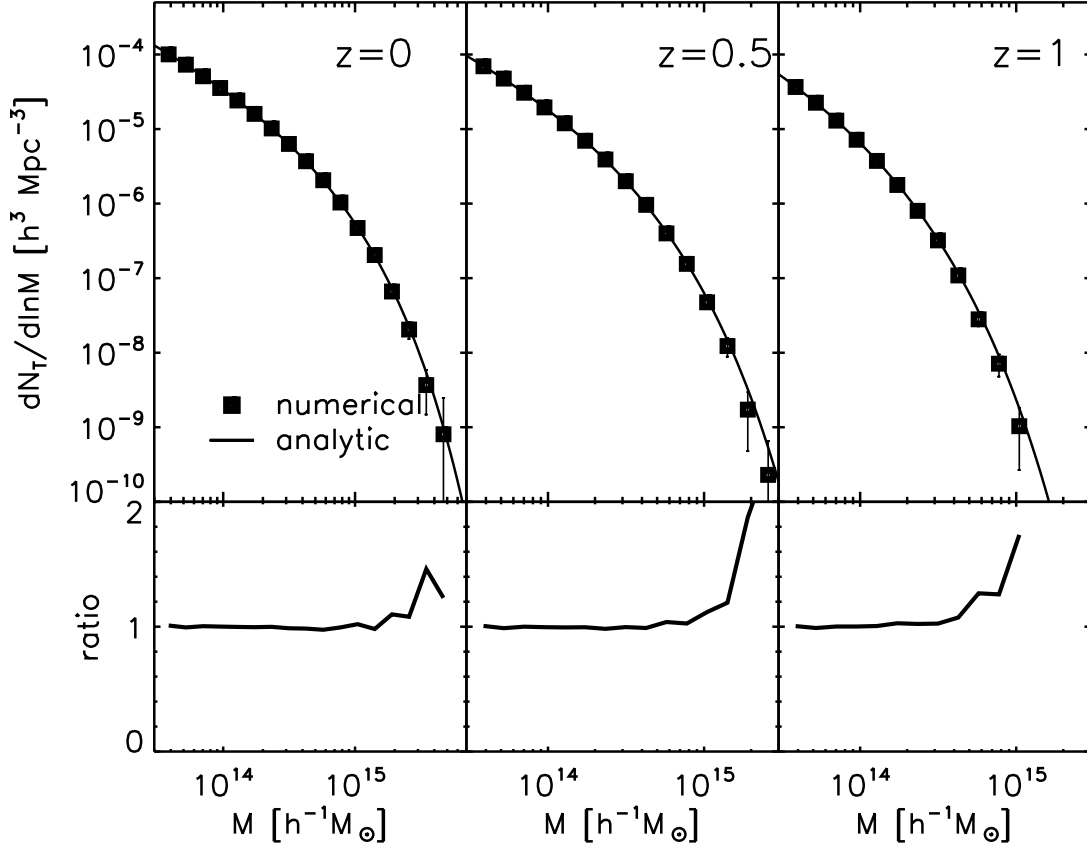


Fig. 1.— Mass function of cluster halos (top panel) and the ratio of the analytic prediction to the numerical result (bottom panel) at $z = 0, 0.5$ and 1 (in the left, middle and right panels, respectively). In each of the top panels the square dots represent the numerical result from the MICE simulations while the solid line is the analytic prediction based on the CA formalism. The errors are the one sigma scatter among the eight Jackknife resamples.

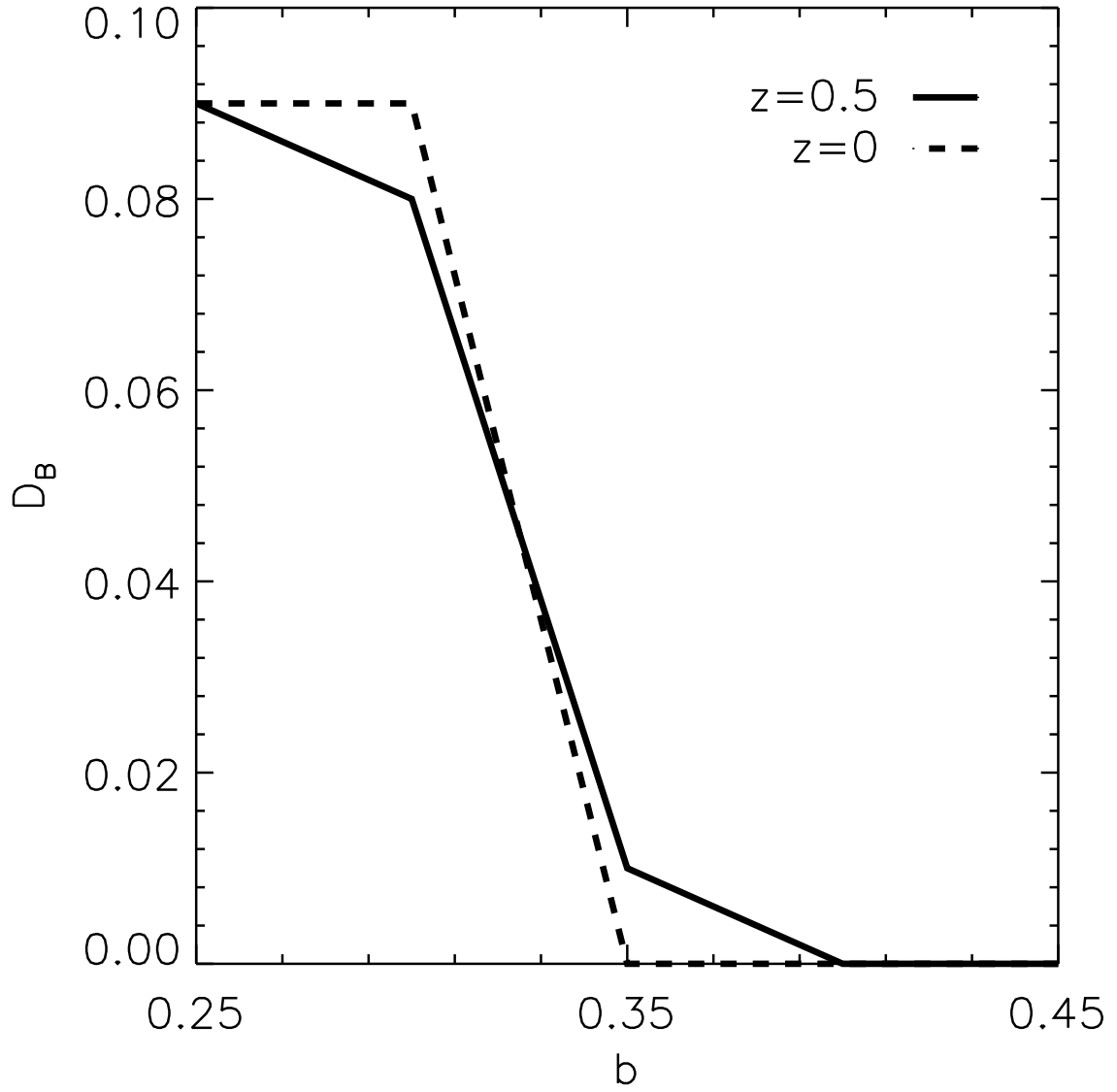


Fig. 2.— Best-fit value of the diffusion coefficient, D_B , versus the linkage parameter, b , used in the FoF algorithm to classify the clusters into the isolated and the non-isolated one at $z = 0$ and 0.5 as dashed and solid lines, respectively. The result at $z = 1$ is very similar to the result at $z = 0.5$.

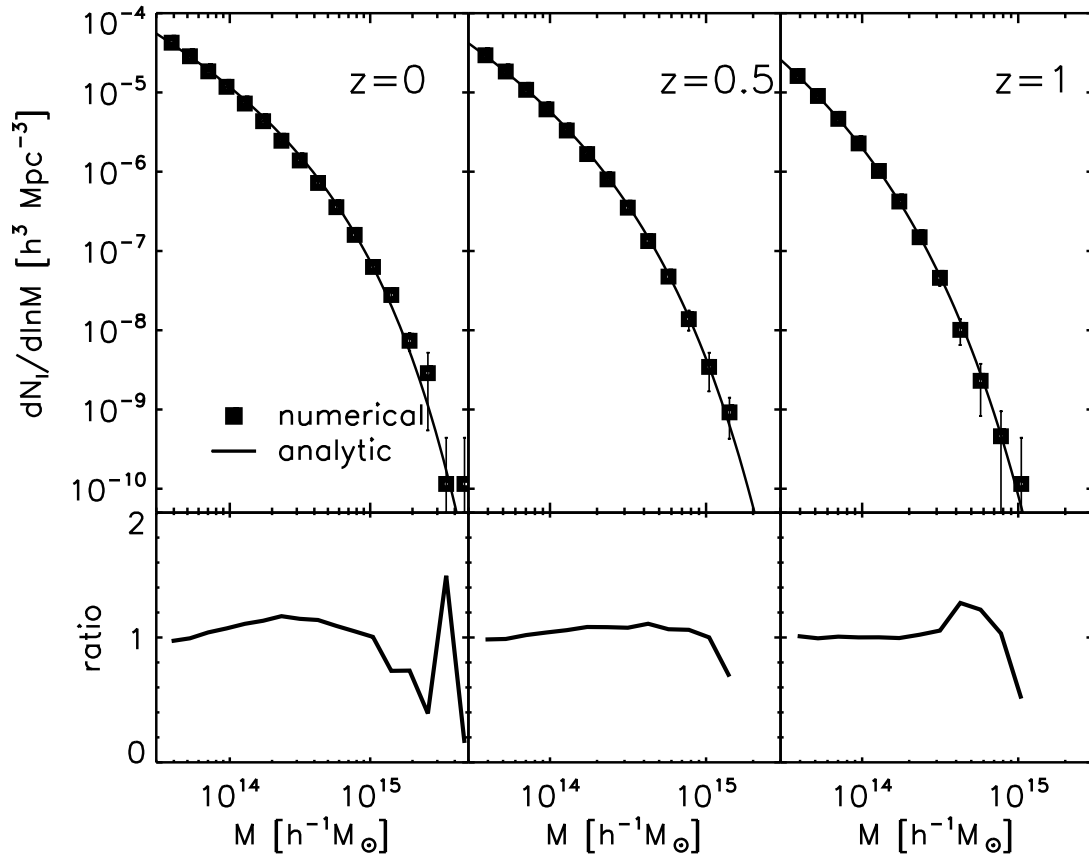


Fig. 3.— Same as Figure 1 but for the isolated cluster halos.

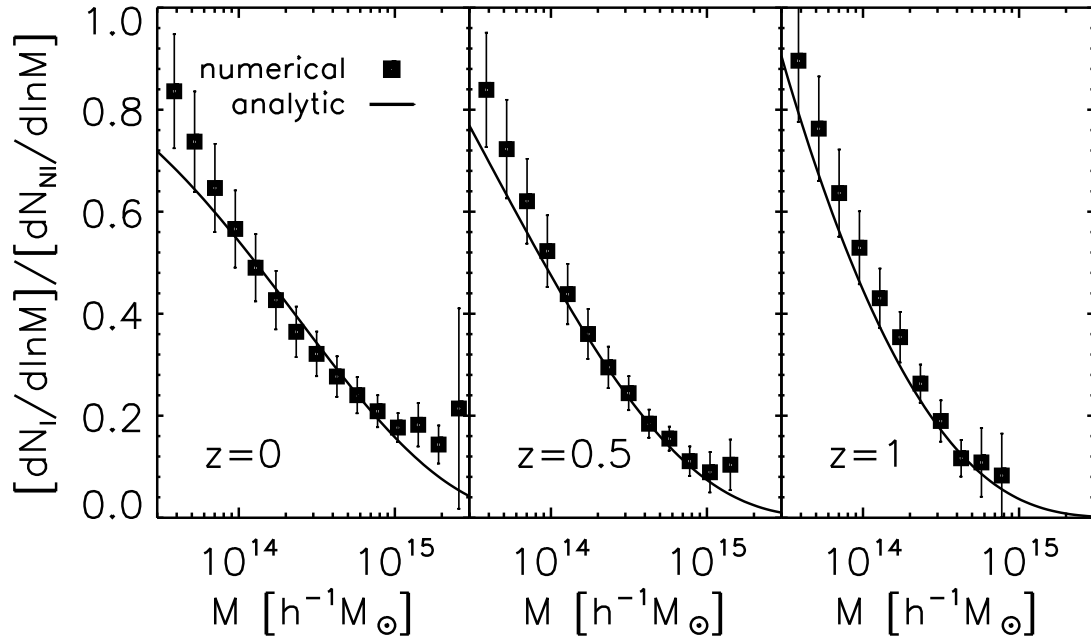


Fig. 4.— Ratio of the mass function of the isolated clusters to that of the non-isolated clusters at $z = 0$, 0.5 and 1 in the left, middle and right panel, respectively.

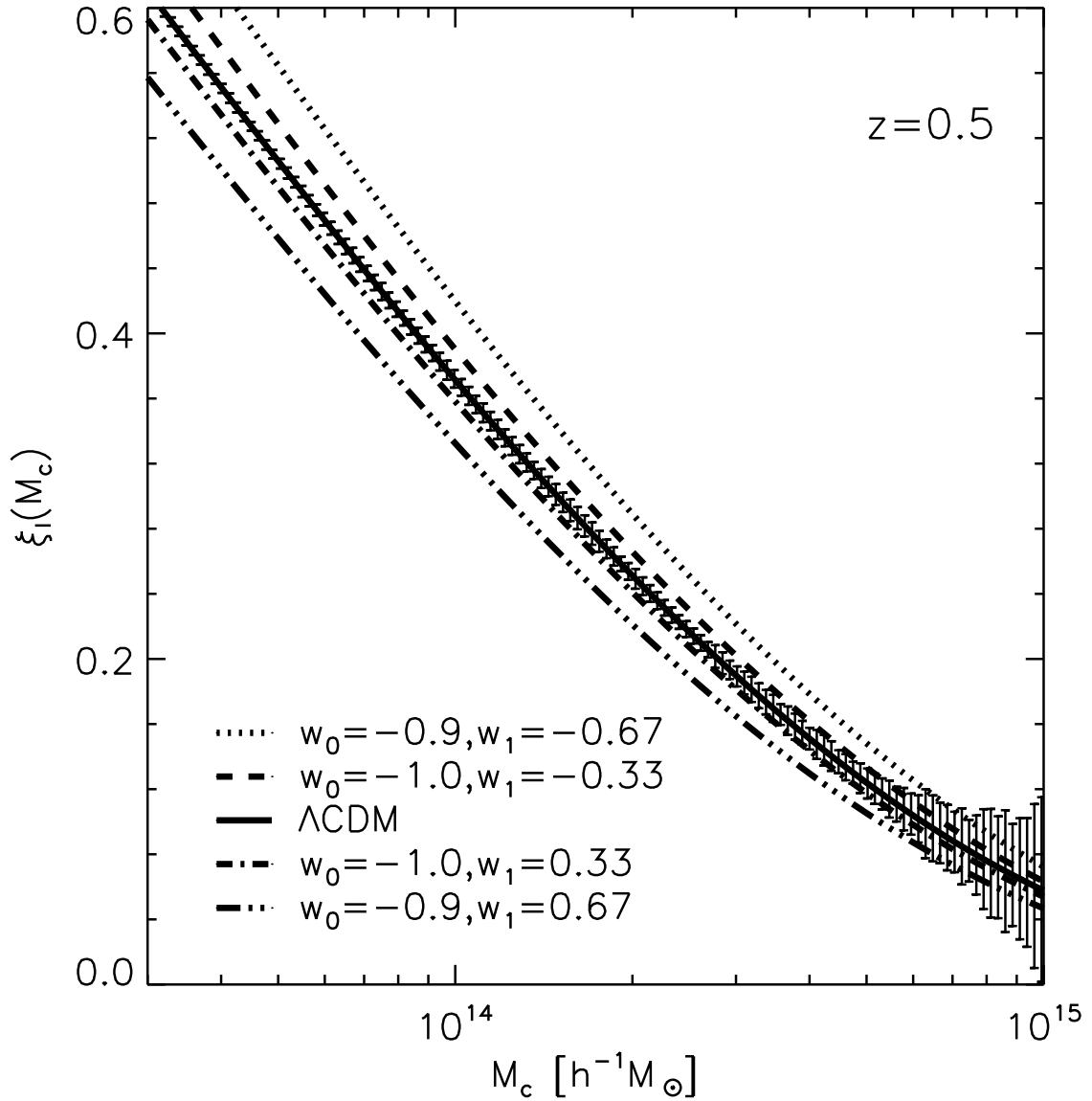


Fig. 5.— Relative abundance of the isolated clusters (Eq. [15]) for five different cases of the dark energy equation of state: $w(z) = w_0 + w_1 z / (1 + z)$. The errors for the ΛCDM -case are obtained as the one σ scatter among the eight Jackknife resamples.

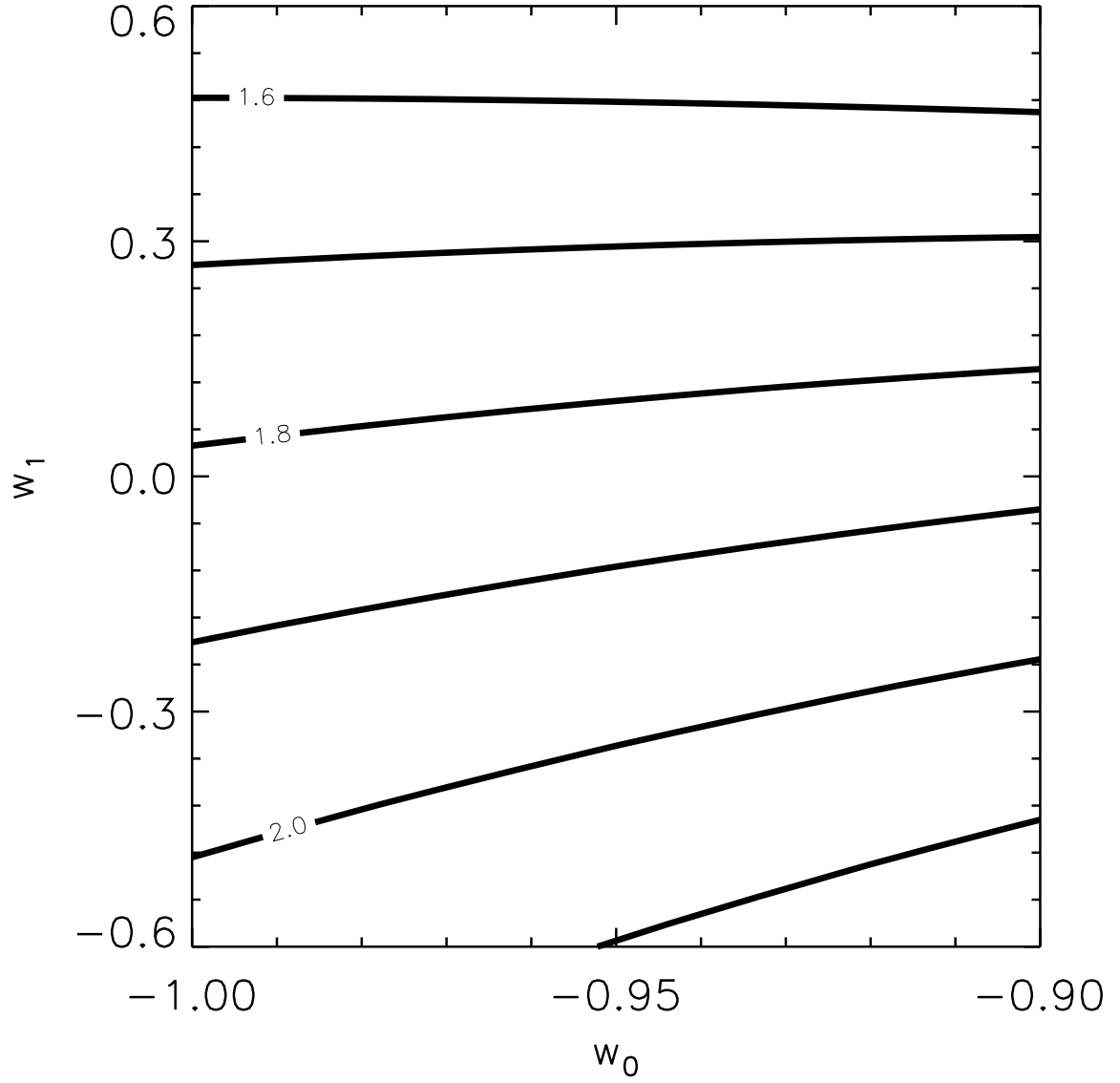


Fig. 6.— Contour plot for the relative abundance of the isolated clusters at $z = 0.5$ in the w_0 - w_1 plane.

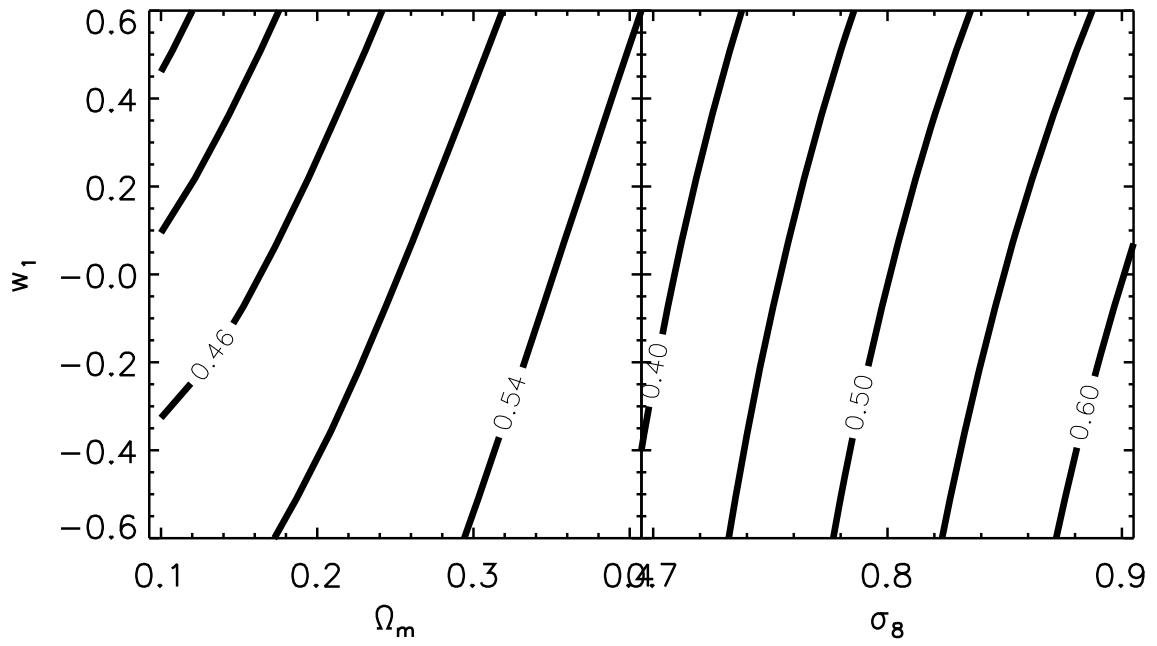


Fig. 7.— Contour plot for the relative abundance of the isolated clusters at $z = 0.5$ in the Ω_m - w_1 plane (left panel) and in the σ_8 - w_1 plane (right panel).

Table 1. Redshift, total number of clusters, and best-fit values of the two coefficients in the CA11 formalism.

z	N_{T}	D_B	β
0	2819031	0.38	0.107
0.5	1684018	0.38	0.095
1	749614	0.38	0.078

Table 2. Redshift, number of isolated clusters, and best-fit values of the two coefficients in the CA formalism

z	N_{I}	D_B	β
0	1334200	0.0	0.34
0.5	782254	0.0	0.20
1	358073	0.0	0.08